Estimation of grain boundary segregation enthalpy and its role in stable nanocrystalline alloy design

Citation: Murdoch, Heather A., and Christopher A. Schuh. "Estimation of grain boundary segregation enthalpy and its role in stable nanocrystalline alloy design." Journal of Materials Research 28, no. 16 (August 6, 2013): 2154-2163.

As Published: http://dx.doi.org/10.1557/jmr.2013.211

Publisher: Cambridge University Press (Materials Research Society)

Persistent URL: http://hdl.handle.net/1721.1/80352

Version: Author's final manuscript: final author's manuscript post peer review, without publisher's formatting or copy editing

Estimation of grain boundary segregation enthalpy and its role in stable nanocrystalline alloy design

Heather A. Murdoch[a1], Christopher A. Schuh[a1, c1]

[a1] Department of Materials Science and Engineering, Massachusetts Institute of Technology, Cambridge, Massachusetts 02139

Abstract

Grain boundary segregation provides a method for stabilization of nanocrystalline metals – the selection of an alloying element that will segregate to the boundaries can lower the grain boundary energy, attenuating the driving force for grain growth. The segregation strength, relative to mixing enthalpy, of a binary system determines the propensity for segregation stabilization. This relationship has been codified for the design space of positive enthalpy alloys; unfortunately, quantitative values for the grain boundary segregation enthalpy exist in only very few material systems, hampering the prospect of nanocrystalline alloy design. Here we present a Miedema-type model for estimation of grain boundary segregation enthalpy, with which potential nanocrystalline phase-forming alloys can be rapidly screened. Calculations of the necessary enthalpies are made for ~2500 alloys and used to make predictions about nanocrystalline stability.

Abstract Figure: Fig. 1

Keywords: Nanostructure; Grain boundaries; Alloy

[C1] Address all correspondence to this author: e-mail: schuh@mit.edu

I. INTRODUCTION

The segregation of a second element to grain boundaries (GBs) can provide sought-after stabilization of nanocrystalline metals [1-5]. In addition to slowing GB migration kinetics, segregated atoms can perform a primary stabilization function by lowering GB energy, γ. For example, in a dilute solution:

$$\gamma = \gamma_0 - \Gamma(\Delta H^{seg} - kTlog[X]) \quad (1)$$

where γ_0 is the GB energy of the pure (solvent) material, Γ is the solute excess at the GB, ΔH^{seg} is the enthalpy of segregation, and $kTlog[X]$ is the entropic penalty of segregation with kT the thermal energy and X the global solute content.

The enthalpy of grain boundary segregation (ΔH^{seg}) has been measured or calculated via simulation for only a few systems (Table 1), and most often in systems where grain boundary segregation is considered undesirable (i.e. causing GB embrittlement). Conversely, for nanostructure stabilization, segregating alloying additions are specifically desirable, and the important open design question is which elements are best suited to segregate and stabilize the grain boundaries via Eq. (1). In most existing studies of nanostructure stability, the selection of an appropriate alloying element has been based on empirical considerations believed (or assumed) to correlate with GB segregation, including size mismatch [6-10], low bulk solubility [7, 8, 11-15], or cohesive energy [16-18]. However, some of the more successful experimental systems with stabilized nanostructures have relatively modest values of ΔH^{seg}, including Ni-W (ΔH^{seg} ~ 10 kJ/mol) [19, 20] and Pd-Zr (ΔH^{seg} ~ 31 kJ/mol) [21]. Regardless of the value of ΔH^{seg}, there is often another problem with the nanostructural stability— precipitation of a second phase, which

disrupts the segregation state necessary for stability and thus triggers grain coarsening [6, 11, 16, 22-28].

It has been a goal of our recent work to identify GB segregation states in nanostructured materials that are formally stable, i.e., not only do they lower GB energy and resist grain growth, but simultaneously oppose second phase precipitation. We have employed a thermodynamic model [29] for a regular nanocrystalline solution (RNS) that incorporates GB segregation [30, 31]. This model describes both grain and grain boundary regions within the nanocrystalline structure and examines the contributions of GB solute segregation to the free energy, while still offering a view of bulk phase separation as a competing condition. In some cases, there exists a segregation state where the excess grain boundary energy can be reduced to zero due to GB segregation, and thus nanocrystalline systems stable with respect to grain growth are possible. In a smaller subset of these cases, the GB-segregated nanocrystalline arrangement is stable against phase separation as well.

A key output of our prior work described above is a preliminary understanding of the characteristic system parameters that favor stable nanostructured systems. For thousands of given sets of parameters defining various binary systems, the effect of GB segregation and grain size on the free energy across a full global composition range was explored and assessed according to the stability criteria [31]. The significant parameters in the RNS model can be directly related to two enthalpies – the bulk crystalline interaction parameter, ω_c, is proportional to ΔH^{mix}, while the pure interfacial energies (γ_A and γ_B), ω_c, and the GB interaction parameter (ω_{gb}), contribute directly to ΔH^{seg}. The full segregation enthalpy from the RNS equilibrium condition [29, 31] includes composition and grain size dependencies in addition to the materials parameters of ω_{gb},

etc. Simplifying this relation to the dilute limit (denoted by subscript 0), we distill the segregation enthalpy to its essential characteristic parameters:

$$\Delta H_0^{seg} = z\left[\omega_c - \frac{\omega_{gb}}{2} - \frac{\Omega_B\gamma_B - \Omega_A\gamma_A}{2zt}\right] \quad (2)$$

The behavior of a material system is thus defined by the parameters embodied in the mixing and dilute segregation enthalpy.

For positive enthalpy of mixing systems, our results suggest that, at a constant reduced temperature (fraction of the critical temperature, $T_{cr} = \Delta H^{mix}/2R$, representing the apex of the miscibility gap with ΔH^{mix} the heat of mixing and R the gas constant), stability can be attained when the following inequality is satisfied [31]:

$$\frac{\Delta H_0^{seg}}{(\Delta H^{mix})^a} > c \quad (3)$$

Here *a* and *c* are temperature dependent constants which we have empirically established through a series of numerical calculations.

As Eq. (3) suggests, we have concluded that the absolute magnitude of the GB segregation enthalpy is not as important as its relation to mixing enthalpy; the two halves of this problem (bulk mixing and GB segregation) must both be considered together to arrive at a reasonably predictive design methodology. Therefore, a strong estimate of the GB segregation enthalpy is necessary, and yet, as noted above, this quantity is not well known for most binary systems.

As in the Fowler-Guggenheim (F-G) segregation form, solute-solute interactions in the grain boundary are explicitly included through the use of a separate GB interaction parameter. In

F-G, this GB interaction is usually quantified for a material system by fitting experimental data [32, 33] – it is not a known parameter. Similarly, while other RNS model parameters are more readily linked to materials properties, the GB interactions codified by ω_{gb} are unknown a priori. As we are seeking to use Eq. (3) and its attendant method [31] in a predictive capacity, we therefore seek a predictive model for GB segregation. Additionally, a direct analog to Eq. (2) is what is necessary to utilize the relation of Eq. (3) for predicting stable nanocrystalline alloys.

We discussed this issue briefly in a recent short report [30], and provided an approximation for ΔH_0^{seg} that allowed us to approach the binary alloy design problem in one specific system (W-based alloys). It is our purpose in this article to expand upon the ideas in that preliminary report and discuss their broader applicability to binary metallic systems in general. In what follows, we first examine previous descriptions of interfacial segregation enthalpy, en route to presenting a new, simple analytical model for GB segregation. This model, while still an analytical approximation for the very complex problem of GB segregation, permits progress on the design of stable nanocrystalline alloys.

II. MODELING OF GB SEGREGATION

A. Prior Segregation Models

Among all the possible binary metal pairs that may be of interest in designing nanostructured materials, very few experimental measurements or atomistic modeling predictions of GB segregation enthalpies exist. In fact, literature values of these quantities are presented in Table 1, and the systems represented comprise less than 1% of those that are possible. General models to predict the propensity for grain boundary segregation include those

of Hondros and Seah [34, 35], McLean [36], Wynblatt and Ku [37], and Darling et al. [38]. These are briefly detailed in what follows.

- Hondros and Seah used experimental segregation data predominantly for impurities in steel to create a rough estimate of the enthalpy of segregation that is directly correlated to the bulk solute solubility, X_{sol}, of the alloy system:

$$\Delta H_{H-S}^{seg} = RTLog[X_{sol}] - 10 \pm 6kJ/mol \quad (4)$$

  This correlation is strictly empirical, and based on a very limited range of alloys. The physical validity of bulk solubility as an indicator of GB segregation is also questionable [39], as X_{sol} derives from bulk phase equilibria considerations and does not speak to the energetics of grain boundaries – this segregation enthalpy essentially relies entirely on mixing enthalpy.

- McLean developed a model for the case where elastic energy is the driving force for solute segregation to the grain boundary, i.e., where GB segregation occurs only to relieve size mismatch strain energy. The elastic strain energy change can be written using an Eshelby-type continuum linear elastic formalism to describe the energy change of substituting a solute atom for a solvent atom in the matrix [40]. McLean further assumed this elastic enthalpy to be fully released by GB solute segregation:

$$\Delta H_{el}^{seg} = \Delta E_{el} = \frac{24\pi K_A G_B r_B r_A (r_B - r_A)^2}{3K_A r_A + 4G_B r_B} \quad (5)$$

  Here, the solute is denoted by subscript B and solvent by subscript A; *K* is bulk modulus, *G* is shear modulus, *r* is the atomic radius. This term is always positive,

which means it will predict that a solute will segregate to the grain boundary in all cases.

- The Wynblatt-Ku model for surface segregation combines both the elastic mismatch with chemical and interfacial energy contributions; the difference in interfacial energies, γ^S, and the area per mole of the interface, $\sigma = N_{avg} V_B^{2/3}$ is described by the first term of Eq. (6):

$$\Delta H_{W-K}^{seg} = (\gamma_B^S - \gamma_A^S)\sigma + 2\omega_c \left[z^l (x - x^s) + z^v \left(x - \frac{1}{2} \right) \right] - \Delta E_{el} \qquad (6)$$

while the second term describes the chemical interactions, where ω_c is the bulk crystalline interatomic interaction parameter and *z*, the total coordination number of the system, is split into in-plane, z^l , and out of plane, z^v, coordination through the following relation: $z = z^l + 2z^v$. It has been suggested that the elastic term needs no modification to be used in both surface and grain boundary segregation [41], provided that the original complete-relaxation assumption of McLean is deemed acceptable. However, Darling and coworkers suggested a modifying parameter, α, to the chemical and interfacial terms to account for the difference between free surfaces and grain boundaries. Specifically, α is the ratio between interfacial and surface strengths (taken in their work as 5/6 to reflect the assumption of $\gamma \approx 1/3\, \gamma^S$ [8]), and their adaptation of Eq. 6 is written [38]:

$$\Delta H_D^{seg} = (\gamma_B^S - \gamma_A^S)(1 - \alpha)\sigma - \frac{8\Delta H_{mix}}{z} \left[z^l (x^s - x) - z^v \left(x - \frac{1}{2} \right) + \alpha \left(x^s - \frac{1}{2} \right) - \right] - \Delta E_{el} \qquad (7)$$

Darling and coworkers showed that this approach is useful for comparing the segregation efficacy of possible solute choices at a fixed composition. However, it is not suitable for our purposes of modeling nanostructure stability because it does not give a segregation enthalpy independent of grain boundary solute content, nor can it be taken to the dilute limit to arrive at a dilute ΔH_0^{seg} for, e.g., use with Eq. (2).

B. Miedema-Based Grain Boundary Segregation Model

What is broadly needed in order to predict and design stable nanocrystalline alloys , i.e., in order to use Eq. (3) and the associated analytical apparatus of our prior work [30, 31], is a means of screening many alloy combinations in the two variables ΔH^{mix} and ΔH_0^{seg}. Each of these parameters can be calculated to great precision using, e.g., atomistic methods. For GB segregation, for example, segregation enthalpies for solutes at specific boundaries [42-45], or even average quantities for ensembles of many boundaries [46-48], can be calculated. Clearly for specific systems of interest this is the most rigorous approach available at present. However, progress on the broader design problem requires that we make decisions about what systems to pursue in the absence of such rigorous data. We require a more exhaustive set of values for ΔH_0^{seg}, and the paucity of available data is such that accuracy can be compromised in the spirit of rapid screening. This situation is reminiscent of the earlier one in bulk alloy theory, where the semi-empirical model of Miedema provided a quick, reasonably accurate description of alloy thermodynamic parameters to allow good estimations without the need for lengthy calculations [49, 50]. For many systems, Miedema estimates of, e.g., ΔH^{mix} and compound formation energies,

are still sufficiently accurate to be widely used for design and analysis. For solid solutions, the Miedema enthalpy of mixing is written [49, 50]:

$$\Delta H_{s.s.}^{mix} = \left[c_A c_B (c_B^s \Delta H_{AinB}^{int} + c_A^s \Delta H_{BinA}^{int})\right]_{chemical} + \left[c_A c_B (c_B \Delta H_{AinB}^{elastic} + c_A \Delta H_{BinA}^{elastic})\right]_{elastic} + \Delta H_{s.s.}^{structural} \quad (8)$$

where c_A and c_B are the compositions of solute and solvent and c_A^s and c_B^s are effective fractions of the surface of A atoms in contact with B atoms and vice versa. This describes the difference in interaction between a B atom surrounded by A atoms, and one surrounded by some mixture of A and B atoms, dictated by composition. Chemical interactions are captured by the terms of form ΔH_{BinA}^{int}, which describe, e.g., the enthalpy of a B atom completely surrounded by A atoms.

Inspired by the prior success of the Miedema model for bulk thermodynamics, we have adopted the same approach for rapidly tabulating GB segregration enthalpies. In a similar spirit to the Wynblatt-Ku adaptation of surface segregation to the case of grain boundaries reviewed above [37, 38], we adapt Miedema's model for surface segregation [49-51] to the grain boundary environment. Miedema's model for dilute surface segregation [51] includes both a chemical interaction enthalpy, ΔH_{BinA}^{int}, and interfacial energy terms which together describe the chemical and interfacial driving forces for segregation that are mirrored in the previously discussed models for segregation:

$$\Delta H_{0,Mied}^{seg} = 0.71 * \frac{1}{3} * [-\Delta H_{BinA}^{int} - c_0 \gamma_A^S V_A^{2/3} + c_0 \gamma_B^S V_B^{2/3}] \quad (9)$$

the term $c_0 \gamma^S V^{2/3}$ is the surface enthalpy of a pure metal as defined by Miedema, where c_0 = 4.5x10^8 is a dimensionless semi-empirical constant, V is atomic volume, and γ^S is surface energy of the pure subscripted component. The coefficient $\frac{1}{3}$ captures the change in coordination at the

surface; when the segregant B atom is at the surface rather than in the bulk, it has gone from being surrounded by A atoms to being only two-thirds in contact. With this fractional contact, $\frac{1}{3}$ of the interaction energy ($\frac{1}{3}\Delta H_{BinA}^{int}$) and one third of the surface ($\frac{1}{3}c_0\gamma_A^S V_A^{2/3}$) is lost, but one third of the new surface is now B ($+\frac{1}{3}c_0\gamma_B^S V_B^{2/3}$).The coefficient 0.71, calibrated by Miedema [51], describes the surface relaxation due to surface electron density distribution and surface geometry which reduces the exposed surface area.

In the case of a grain boundary, the basic approach of Miedema as captured in Eq. (9) remains valid, but requires some corrections. A first correction pertains to the coordination of atoms at grain boundaries, which led to the coefficient of 1/3 in Eq. (9). As formulated by Trelewicz, the regular nanocrystalline solution model for nanocrystalline alloys involves an accounting of bonds in the bulk, in the grain boundary region, and "transition" bonds that connect those two regions. An atom relocated from bulk to boundary would lose 1/3 of its bulk contact, as before, but would be coordinated by other atoms in the adjoining grain. Only a fraction of those bonds, defined by Trelewicz as ν (and assigned a value of ½ applicable for most all grain sizes) would therefore be lost [29]. A second correction is to introduce the elastic term, Eq. (5), to account for the elastic strain effects that contribute to segregation which are missing from Miedema's model. With these modifications, we arrive at the following model for the dilute grain boundary segregation enthalpy:

$$\Delta H_{0,M}^{seg} = -0.71 * \frac{1}{3} * \nu * \left[-\Delta H_{BinA}^{int} - c_0\gamma_A^S V_A^{\frac{2}{3}} + c_0\gamma_B^S V_B^{\frac{2}{3}}\right] + \Delta E_{el} \qquad (10)$$

Note that the sign convention in Eq. (10) is reversed from that of the original Miedema model in Eq. (9), to match the convention of the RNS model, where a positive value of

segregation enthalpy denotes propensity for grain boundary segregation. Equation (10) requires no temperature and composition assumptions, contains readily available materials data, and describes dilute segregation – all the requirements outlined earlier as needed for predicting nanocrystalline alloy stability.

III. GRAIN BOUNDARY SEGREGATION CALCULATIONS

The dilute GB segregation enthalpy was calculated using Eq. (10) for approximately 2500 binary alloys, where data was available. The first pass calculation for all alloys was using the readily available Miedema terms [49, 50]. The resulting segregation energy is denoted in Fig 1 by a solid color – red for GB-segregating solutes and blue for anti-segregating (that is, the GB will be enriched by *solvent*, with the solute preferring the grain interior), scaled by strength. Whenever possible, we validated Miedema's prediction for the chemical interaction term through comparison with other sources of thermodynamic data. Additionally, when a Miedema calculation of ΔH_{BinA}^{int} was not available for a particular binary system, or did not physically match the most basic expectations for the material system (e.g. predicted a strongly negative interaction for a system with no known ordered compounds), only other sources of data are used and presented in Fig. 1. Calculations with secondary sources are indicated in the figure by a dot. If both Miedema values and secondary sources were used to make the calculation, the square is bisected with the upper, solid half representing Miedema values, and the lower half showing the output based on secondary sources. A fully blacked-out square indicates that we did not find suitable data to make the calculation.

The most common source of secondary data is a Redlich-Kister-Muggianu (RKM) style model for a solid solution used for CALPHAD phase diagram calculations [52]:

$$\Delta H_{RKM}^{mix} = X_i X_j \sum_v L_v^{ij} \left(X_i - X_j\right)^v \quad (11)$$

with X_i and X_j the components of the binary system and L_v the vth fitted binary interaction parameter in the expansion. This is a full enthalpy of mixing, fitted to experimental data, thus necessarily encompassing all contributions to enthalpy, i.e. chemical and elastic. To extract the ΔH_{BinA}^{int}term necessary for the segregation calculation of Eq. (10) from an RKM model, it is set equal to the Miedema mixing enthalpy model, Eq. (8). The critical temperature, T_{cr}, which is necessary for the application of the predictive enthalpy relation, Eq. (3), must also be calculated. In a symmetric regular solution the top of the miscibility gap simply equals $\Delta H^{mix}/2R$; for RKM models, asymmetry and/or temperature dependencies in the coefficients require a more elaborate method to calculate T_{cr} by examining the free energy as a function of temperature. In some cases, the RKM fit results in a highly skewed, unreasonable temperature-dependent enthalpy. In these cases, our ability to extract a comparable chemical interaction term for use in Eq. (10) is questionable; an "x" indicates such systems in Fig. 1. The numerical results of these calculations are in the supplemental material.

The results in Fig. 1 are interesting for their potential use in screening systems for stable nanocrystalline states, and we will turn our attention to this issue in the next section. However, it is first interesting to examine some features of the data set.

Knowing that both bulk alloy and grain boundary thermodynamics derive from the same chemical interactions among the alloy species, one might expect that ΔH^{mix} and $\Delta H_{0,M}^{seg}$would be correlated in some way. And while these parameters are formally independent, it is interesting to examine the space of calculated outputs for the ~2500 alloys considered in this study. Figure 2 shows a survey of the two quantities in relation to one another for the alloys explored here. We

note that the design space is quite thoroughly covered by these alloy pairs. This result supports the criticism of the empirical Hondros-Seah relation of Eq. (4), which attempts to estimate GB segregation enthalpy based only on bulk thermodynamics; Fig. 2 shows that the one does not well correlate with the other. Additionally, our design space covers negative, or anti-segregating, values of segregation enthalpy, which the Hondros-Seah and McLean models cannot.

The departure of our model from prior approaches can be more easily visualized in Fig. 3, where our predicted values of $\Delta H_{0,M}^{seg}$ are compared to those predicted by the Hondros-Seah equation (Eq. (4)) and the McLean elastic-only model (Eq. (5)). (Direct comparisons are not possible to the Wynblatt-Ku and Darling models without making assumptions about GB solute concentration.) Several features are of interest in this figure. First, as expected, there is no correlation between our segregation enthalpy model and the solubility-based model of Hondros and Seah (Fig. 3). Because the elastic enthalpy is a component of our model, there is a positive correlation between $\Delta H_{0,M}^{seg}$ and ΔH_{el}^{seg}, but it is a sufficiently weak correlation to be of limited practical use. The chemical and interfacial components included here are quantitatively as important as the elastic mismatch for grain boundary segregation.

Second, in both cases, the present Miedema model $\Delta H_{0,M}^{seg}$ predicts cases where an alloy would be anti-segregating (negative values) where ΔH_{H-S}^{seg} and ΔH_{el}^{seg} are only able to return positive values. The number of negative values in Figs. 1 and 2 suggest that such cases may be common, and could therefore be of practical importance. For example, in the Cu-Ni system, atomistic modeling shows depletion of nickel at the GBs compared to the bulk [53] with a segregation energy of -7 kJ/mol. This matches extremely well with the present estimation of

$\Delta H_{0,M}^{seg}$ = -8 kJ/mol, but diverges substantially from the elastic enthalpy prediction, ΔH_{el}^{seg}, which is very low but still positive at 0.6 kJ/mol, and the Hondros-Seah prediction of 21-33 kJ.

As noted in the introduction, the number of quantitative measurements of ΔH^{seg} based on experiment or computational modeling are few, but a comparison of the present predictions with available measurements is included in Table 1. It should be noted that Eq. (10) is a dilute-limit segregation enthalpy, which complicates the comparison to systems at non-dilute concentrations. Nonetheless, the general agreement between Eq. (10) and the available independent measurements is reasonable. In about half of the cases, the values are a close match to one another. The other half range from reasonable (e.g., within a factor of two) to poor matches. Some of the most conspicuous disagreements include systems like Fe-Sn, Ni-In, Co-Sb, which involve elements outside of the central transition metal block, for which electronic and structure effects may be more complex than are adequately handled by the Miedema approach.

IV. NANOCRYSTALLINE ALLOY SCREENING

Our goal is to make predictions about the ability of a binary alloy system to support a nanocrystalline state through solute-stabilized GBs. The two quantities of Eq. (3) comprise the axes of an alloy screening space, upon which we can define a stability map. We presented the construction of these maps in Refs. [30, 31], and here take the additional step of quantitatively placing alloy systems on the maps. For simplicity, the discussion here is limited to systems with positive heats of mixing and GB segregation, which matches our prior developments in Ref. [31]. We use the results of our segregation model combined with data sources for ΔH^{mix}, as presented in Fig. 4 for five reduced temperatures.

In these maps, the lowest, red, region represents the enthalpy-space in which no stable nanocrystalline states are supported. In this region, the system ground state is a coarse-grained structure with phases given by the bulk phase diagram. This is also the ground state in the middle, yellow, region, but in this space there exist nanocrystalline states that are stable against grain growth, but not against phase separation. The top, green, regions of each map describe the design space in which nanocrystalline states exist with complete stability. A given base element solvent is assigned a specific symbol, and the solute element is labeled on the map next to the symbol. For example, copper-based alloys are indicated by a solid blue circle; the Cu-Ag alloy specifically is represented by this blue circle, labeled by "Ag".

Only Miedema sources of chemical interaction data are presented in this figure for simplicity, with the exception of a handful of alloys we wish to highlight to connect with systems in which nanocrystalline stability has been experimentally evaluated. These alloys are listed in Table 2 and indicated on the maps in Fig. 4 by larger labels, and are both in italics and underlined if their calculation used sources alternate to Miedema's tables of ΔH_{BinA}^{int}. Table 2 is arranged according to the degree of predicted stability. The segregation model predicts a stable nanostructured state in W-Ti (for details, see [30]); metastable for W-Cu, Fe-Ag, Fe-Cu, Cu-Bi, and Cu-Pb; and not stable for Cu-Ag, Ag-Cu, Al-Pb, Au-Ni, and Ni-Cu. In the metastable cases, the thermodynamically stable phase is a coarse-grained phase separated structure, but appropriate segregation opposes the driving force for grain growth. For example, in a solid solution nanocrystalline W-Cu alloy, the nanostructure is retained after annealing at 673K for one hour, but subsequent annealing triggers phase separation, leading to rampant grain growth [54]. For Fe-Ag[16, 55], the Ag-rich phase precipitated at 673K after one hour and also at room temperature after four weeks, showing that the equilibrium phases are indeed dictated by the bulk miscibility gap.

Minimal grain growth was reported before bulk phase separation in Fe-Cu [26], after which the grains grew rapidly. In the Cu-Bi system, thermal stability is improved dramatically relative to pure nc-Cu [7] and grains grew after annealing above 433K.

For an example unstable case, that of Cu-Ag, phase separation and rampant grain growth was observed experimentally in an initially-nanocrystalline solid solution [56] and atomistic modeling concluded that silver was not sufficient to significantly lower the energy of the GBs [57]. For an Al-Pb alloy, two phases were still present even after extensive mechanical alloying to a nanostructured state [58]; modeling showed that Pb segregated to the GBs , then formed clusters [47]. The local enthalpy at the GBs was significantly lowered by the placement of Pb atoms of GB sites; however, this atom placement raised the global enthalpy substantially, indicating a non-equilibrated state [47]. Annealing of nanocrystalline Au-Ni for one hour at 673K resulted in complete phase separation [27]; phase separation was also observed at 473K, but not completed within one hour. A Cu-rich phase precipitated from a nanocrystalline Ni-Cu alloy when annealing temperatures exceeded 525K – after three hours at 575K, the material was 15%Cu phase [59].

These observations thus qualitatively align with the predictions of the model. While it is very difficult to determine true metastability or instability from the experimental studies, the general agreement is encouraging. It is noteworthy that this agreement is better than can be attained using prior methods for estimating ΔH^{seg}. These methods routinely overpredict segregation enthalpy, and would therefore expect stability in the majority of the experimental alloys described above.

V. CONCLUSIONS

We have presented a model with which the dilute-limit grain boundary segregation enthalpy can be estimated in metal alloy pairs. The approach can be used in conjunction with nanocrystalline stability maps to predict the nanocrystalline stability of hundreds of binary alloys. This segregation model is built upon Miedema's model for surface segregation, adapted to the GB environment. While not presenting a detailed picture of GB segregation, it allows for quick calculations across a large range of alloys; this, in turn, enables a broad population of the stable nanocrystalline design space. Predictions of stability in existing experimentally studied systems are briefly evaluated, with good agreement.

ACKNOWLEDGEMENTS

This research was supported primarily by the U.S. Army Research Office under contract W911NF-09-1-0422, with partial additional support from the Solid State Solar Thermal Energy Conversion (S3TEC), an Energy Frontier Research Center funded by the U.S. Department of Energy, Office of Science, Office of Basic Energy Sciences under DE-SC0001299.

REFERENCES

1. J. Weissmüller: Alloy effects in nanostructures. *Nanostruct. Mater.* **3**(1-6), 261. (1993)
2. J. Weissmüller: Some basic notions on nanostructured solids. *Mater. Sci. Eng., A* **179-180**(Part 1), 102. (1994)
3. R. Kirchheim: Grain coarsening inhibited by solute segregation. *Acta Mater.* **50**(2), 413. (2002)
4. F. Liu and R. Kirchheim: Nano-scale grain growth inhibited by reducing grain boundary energy through solute segregation. *J. Cryst. Growth* **264**(1-3), 385. (2004)
5. R. Kirchheim: Reducing grain boundary, dislocation line and vacancy formation energies by solute segregation. I. Theoretical background. *Acta Mater.* **55**(15), 5129. (2007)
6. J. Weissmüller, W. Krauss, T. Haubold, R. Birringer, and H. Gleiter: Atomic structure and thermal stability of nanostructured Y-Fe alloys. *Nanostruct. Mater.* **1**(6), 439. (1992)
7. X. Chen and J. Mao: Thermal stability and tensile properties of electrodeposited Cu-Bi alloy. *J. Mater. Eng. Perform.* **20**(3), 481. (2011)
8. K.A. Darling, B.K. VanLeeuwen, C.C. Koch, and R.O. Scattergood: Thermal stability of nanocrystalline Fe-Zr alloys. *Mater. Sci. Eng., A* **527**(15), 3572.
9. C.E. Krill, H. Ehrhardt, and R. Birringer: Thermodynamic stabilization of nanocrystallinity. *Z. Metallk.* **96**(10), 1134. (2005)
10. M. Atwater, H. Bahmanpour, R. Scattergood, and C. Koch: The thermal stability of nanocrystalline cartridge brass and the effect of zirconium additions. *J Mater Sci* 1. (2012)
11. P. Choi, M. da Silva, U. Klement, T. Al-Kassab, and R. Kirchheim: Thermal stability of electrodeposited nanocrystalline Co-1.1at.%P. *Acta Mater.* **53**(16), 4473. (2005)
12. M.A. Atwater, D. Roy, K.A. Darling, B.G. Butler, R.O. Scattergood, and C.C. Koch: The thermal stability of nanocrystalline copper cryogenically milled with tungsten. *Mater. Sci. Eng., A* **558**(0), 226. (2012)
13. M.A. Atwater, R.O. Scattergood, and C.C. Koch: The stabilization of nanocrystalline copper by zirconium. *Mater. Sci. Eng., A* **559**(0), 250. (2013)
14. D. Osmola, P. Nolan, U. Erb, G. Palumbo, and K.T. Aust: Microstructural evolution at large driving forces during grain growth of ultrafine-grained Ni–1.2wt%P. *Phys. Status Solidi A* **131**(2), 569. (1992)
15. A.A. Talin, E.A. Marquis, S.H. Goods, J.J. Kelly, and M.K. Miller: Thermal stability of Ni-Mn electrodeposits. *Acta Mater.* **54**(7), 1935. (2006)
16. F. Liu: Grain growth in nanocrystalline Fe-Ag thin film. *Mater. Lett.* **59**(11), 1458. (2005)
17. E. Pellicer, A. Varea, K.M. Sivaraman, S. Pane, S. Surinach, M. Dolors Baro, J. Nogues, B.J. Nelson, and J. Sort: Grain Boundary Segregation and Interdiffusion Effects in Nickel-Copper Alloys: An Effective Means to Improve the Thermal Stability of Nanocrystalline Nickel. *ACS Appl. Mater. Inter.* **3**(7). (2011)
18. Y.R. Abe, J.C. Holzer, and W.L. Johnson FORMATION AND STABILITY OF NANOCRYSTALLINE NB-CU ALLOYS in Structure and Properties of Interfaces in Materials (Mater. Res. Soc. Symp. Proc. **238**, Boston, MA 1991), p. 721.
19. A.J. Detor and C.A. Schuh: Grain boundary segregation, chemical ordering and stability of nanocrystalline alloys: Atomistic computer simulations in the Ni–W system. *Acta Mater.* **55**(12), 4221. (2007)
20. A.J. Detor and C.A. Schuh: Microstructural evolution during the heat treatment of nanocrystalline alloys. *J. Mater. Res.* **22**(11), 3233. (2007)
21. B.K. VanLeeuwen, K.A. Darling, C.C. Koch, R.O. Scattergood, and B.G. Butler: Thermal stability of nanocrystalline Pd81Zr19. *Acta Mater.* **58**(12). (2010)
22. M. da Silva, C. Wille, U. Klement, P. Choi, and T. Al-Kassab: Electrodeposited nanocrystalline Co-P alloys: Microstructural characterization and thermal stability. *Mater. Sci. Eng., A* **445-446**31. (2007)

23. B. Färber, E. Cadel, A. Menand, G. Schmitz, and R. Kirchheim: Phosphorus segregation in nanocrystalline Ni-3.6 at.% P alloy investigated with the tomographic atom probe (TAP). *Acta Mater.* **48**(3), 789. (2000)
24. T. Hentschel, D. Isheim, R. Kirchheim, F. Muller, and H. Kreye: Nanocrystalline Ni-3.6 at.% P and its transformation sequence studied by atom-probe field-ion microscopy. *Acta Mater.* **48**(4), 933. (2000)
25. S.C. Mehta, D.A. Smith, and U. Erb: Study of grain growth in electrodeposited nanocrystalline nickel-1.2 wt% phosphorus alloy. *Mater. Sci. Eng., A* **204**(1-2), 227. (1995)
26. J. Eckert, J.C. Holzer, and W.L. Johnson: THERMAL-STABILITY AND GRAIN-GROWTH BEHAVIOR OF MECHANICALLY ALLOYED NANOCRYSTALLINE FE-CU ALLOYS. *J. Appl. Phys.* **73**(1), 131. (1993)
27. E. Rouya, G.R. Stafford, U. Bertocci, J.J. Mallett, R. Schad, M.R. Begley, R.G. Kelly, M.L. Reed, and G. Zangari: Electrodeposition of Metastable Au-Ni Alloys. *J. Electrochem. Soc.* **157**(7), D396. (2010)
28. K.J. Bryden and J.Y. Ying: Thermal stability and hydrogen absorption characteristics of palladium-yttrium nanoalloys. *Acta Mater.* **44**(9), 3847. (1996)
29. J.R. Trelewicz and C.A. Schuh: Grain boundary segregation and thermodynamically stable binary nanocrystalline alloys. *Phys Rev B* **79**(9), 094112. (2009)
30. T. Chookajorn, H.A. Murdoch, and C.A. Schuh: Design of Stable Nanocrystalline Alloys. *Science* **337**(6097), 951. (2012)
31. H.A. Murdoch and C.A. Schuh: Stability of binary nanocrystalline alloys against grain growth and phase separation. *Acta Mater.* **61**(6), 2121. (2013)
32. P. Lejcek and S. Hofmann: Thermodynamic State Functions of Interfacial Segregation and Their Role in the Compensation Effect. *Rev. Adv. Mater. Sci.* **21**(1), 27. (2009)
33. P. Lejcek: Grain Boundary Segregation in Metals. *Grain Boundary Segregation in Metals* **136**. (2010)
34. E.D. Hondros, Seah, M.P.: The Theory of Grain Boundary Segregation in Terms of Surface Adsorption Analogues. *Metall. Trans. A* **8A**1363. (1977)
35. M.P. Seah: Grain boundary segregation. *J. Phys. F: Metal Phys.* **10**(6), 1043. (1980)
36. D. McLean (1957) Grain Boundaries in Metals. Oxford Clarendon Press,
37. P. Wynblatt and D. Chatain: Anisotropy of segregation at grain boundaries and surfaces. *Metall. Mater. Trans. A* **37**(9), 2595. (2006)
38. K.A. Darling, B.K. VanLeeuwen, J.E. Semones, C.C. Koch, R.O. Scattergood, L.J. Kecskes, and S.N. Mathaudhu: Stabilized nanocrystalline iron-based alloys: Guiding efforts in alloy selection. *Mater. Sci. Eng., A* **528**(13-14), 4365. (2011)
39. C.L. Briant: Solid solubility and grain boundary segregation. *Philos. Mag. Lett.* **73**(6). (1996)
40. J. Friedel: Electronic structure of primary solid solutions in metals. *Advances in Physics* **3**(12), 446. (1954)
41. P. Wynblatt and Z. Shi: Relation between grain boundary segregation and grain boundary character in FCC alloys. *J Mater Sci* **40**(11), 2765. (2005)
42. D. Udler and D.N. Seidman: Solute segregation at [001] tilt boundaries in dilute f.c.c. alloys. *Acta Mater.* **46**(4), 1221. (1998)
43. D. Udler and D.N. Seidman: Solute-atom segregation at (002) twist boundaries in dilute Ni□Pt alloys: Structural/chemical relations. *Acta Metall. et Mater.* **42**(6), 1959. (1994)
44. D. Udler and D.N. Seidman: SOLUTE-ATOM SEGREGATION AT HIGH-ANGLE (002) TWIST BOUNDARIES IN DILUTE AU-PT ALLOYS. *J. Mater. Res.* **10**(8), 1933. (1995)
45. O. Duparc, A. Larere, B. Lezzar, O. Khalfallah, and V. Paidar: Comparison of the intergranular segregation for eight dilute binary metallic systems in the Σ 11′ {332} tilt grain boundary. *J Mater Sci* **40**(12), 3169. (2005)

46. Y. Purohit, S. Jang, D.L. Irving, C.W. Padgett, R.O. Scattergood, and D.W. Brenner: Atomistic modeling of the segregation of lead impurities to a grain boundary in an aluminum bicrystalline solid. *Mater. Sci. Eng., A* **493**(1-2), 97. (2008)
47. Y. Purohit, L. Sun, D.L. Irving, R.O. Scattergood, and D.W. Brenner: Computational study of the impurity induced reduction of grain boundary energies in nano- and bi-crystalline Al-Pb alloys. *Mater. Sci. Eng., A* **527**(7-8), 1769.
48. U. Alber, H. Müllejans, and M. Rühle: Bismuth segregation at copper grain boundaries. *Acta Mater.* **47**(15-16), 4047. (1999)
49. H. Bakker (1998) Enthalpies in Alloys: Miedema's Semi-Empirical Model. Trans Tech Publications, Enfield, New Hampshire
50. F.R. de Boer, R. Boom, W.C.M. Mattens, A.R. Miedema, and A.K. Niessen: Cohesion in Metals: Transition Metal Alloys. (1988)
51. A.R. Miedema: SURFACE SEGREGATION IN ALLOYS OF TRANSITION-METALS. *Z. Metallk.* **69**(7), 455. (1978)
52. O. Redlich and A.T. Kister: ALGEBRAIC REPRESENTATION OF THERMODYNAMIC PROPERTIES AND THE CLASSIFICATION OF SOLUTIONS. *Ind. Eng. Chem.* **40**(2), 345. (1948)
53. S.M. Foiles: CALCULATION OF GRAIN-BOUNDARY SEGREGATION IN NI-CU ALLOYS. *Phys Rev B* **40**(17), 11502. (1989)
54. I.H. Moon, S.S. Ryu, S.W. Kim, D.M. Won, and W.S. Jang: Grain growth in the nanocrystalline W-Cu and Cu-Pb composite powders prepared by mechanical alloying. *Z. Metallk.* **92**(8), 986. (2001)
55. F. Liu: Precipitation of a metastable Fe(Ag) solid solution upon annealing of supersaturated Fe(Ag) thin film prepared by pulsed laser deposition. *Appl. Phys. A* **81**(5), 1095. (2005)
56. M. Zhu, Z. Wu, M. Zeng, L. Ouyang, and Y. Gao: Bimodal growth of the nanophases in the dual-phase composites produced by mechanical alloying in immiscible Cu–Ag system. *J Mater Sci* **43**(9), 3259. (2008)
57. S.G. Mayr and D. Bedorf: Stabilization of Cu nanostructures by grain boundary doping with Bi: Experiment versus molecular dynamics simulation. *Phys Rev B* **76**(2), 024111. (2007)
58. Z.F. Wu, M.Q. Zeng, L.Z. Ouyang, X.P. Zhang, and M. Zhu: Ostwald ripening of Pb nanocrystalline phase in mechanically milled Al-Pb alloys and the influence of Cu additive. *Scripta Mater.* **53**(5), 529. (2005)
59. E. Pellicer, A. Varea, S. Pane, B.J. Nelson, E. Menendez, M. Estrader, S. Surinach, M.D. Baro, J. Nogues, and J. Sort: Nanocrystalline Electroplated Cu-Ni: Metallic Thin Films with Enhanced Mechanical Properties and Tunable Magnetic Behavior. *Adv. Funct. Mater.* **20**(6), 983. (2010)
60. Detor: Grain boundary segregation, chemical ordering and stability of nanocrystalline alloys: Atomistic computer simulations in the Ni-W system. *Acta Mater.* **55**4221. (2007)
61. M. Menyhard, M. Yan, and V. Vitek: Atomistic vs phenomenological approaches to grain boundary segregation: Computer modeling of Cu□Ag alloys. *Acta Metall. et Mater.* **42**(8), 2783. (1994)
62. A. Kirchner and B. Kieback: Thermodynamic model of alloy grain boundaries. *Scripta Mater.* **64**(5), 406. (2011)
63. L.S. Chang and K.B. Huang: Temperature dependence of the grain boundary segregation of Bi in Ni polycrystals. *Scripta Mater.* **51**(6), 551. (2004)
64. Z. Chen, F. Liu, X. Yang, C. Shen, and Y. Fan: Analysis of controlled-mechanism of grain growth in undercooled Fe–Cu alloy. *J. Alloys Compd.* **509**(25), 7109. (2011)

Tables

Table 1: Quantitative Comparison of grain boundary segregation energies estimated by the present model and reported based on experiments and simulations in the literature.(Positive values denote a propensity for GB segregation)

Solvent	Solute	$\Delta H_{0,M}^{seg}$ [kJ/mol]	Reported [kJ/mol]	Data Type	Ref.
Ni	Cu	12	14	atomistic – MC EAM	[53]
Cu	Ni	-8	-7	atomistic – MC EAM	[53]
Al	Pb	46	111	atomistic	[46]
Ni	W	9	10	atomistic	[60]
Cu	Ag	18	63	atomistic – MC	[61]
			30	model	[62]
			25,40	experiment	via [33]
			40	experiment	via [62]
Cu	Au	10	10	experiment	via [33]
			~60 (1st layer)	atomistic – MC	[61]
Ag	Ni	10	40	experiment	via [33]
Fe	Si	12	3-17	experiment	via [33]
Fe	Al	29	12	experiment	via [33]
Fe	Cr	4	8	experiment	via [33]
Cu	Bi	83	53	experiment	via [33]
			60-88	experiment	[48]
Ni	Bi	111	117	experiment	[63]
Fe	Cu	19	50-58	model fit to exp.	[64]
Fe	Sn	130	13-23	experiment	via [33]
Ni	In	103	38	experiment	via [33]
Ni	Sb	71	4,63	experiment	via [33]
Co	Sb	76	5	experiment	via [33]
Zr	Cr	69	12	experiment	via [33]
Fe	Ag	58	60-100	model fit to exp.	[16]

Table 2: Nanocrystalline Alloys ($\Delta H^{mix}>0$) whose thermal stability has been tested, and the predicted stability according to Eq. (3). As the coefficients in Eq. (3) have only thus far been calculated for several fractional temperatures, the nearest temperature to experimental values is selected and presented here. Using the figure of merit for the fractional temperature, the nanocrystalline stability of the alloy is predicted, reported through the color of the segregation enthalpy column; the stable alloy is green, metastable are yellow, and unstable are red.

Alloy	**Ref.**	**T [K] of prediction**		$\Delta H_{0,M}^{seg}$ **[kJ/mol]**	
W-Ti	[30]	1373		38	
W-Cu	[54]	726		82	
Cu-Bi	[7, 57]	469		54	
Cu-Pb	[54]	414		30	
Fe-Ag	[16]	768		58	
Fe-Cu	[26]	312	1089	19	19
Cu-Ag	[56]	652		17	
Ag-Cu	[56]	631		12	
Al-Pb	[46, 47, 58]	601		23	
Au-Ni	[27]	390		16	
Ni-Cu	[17]	548		12	

Figures

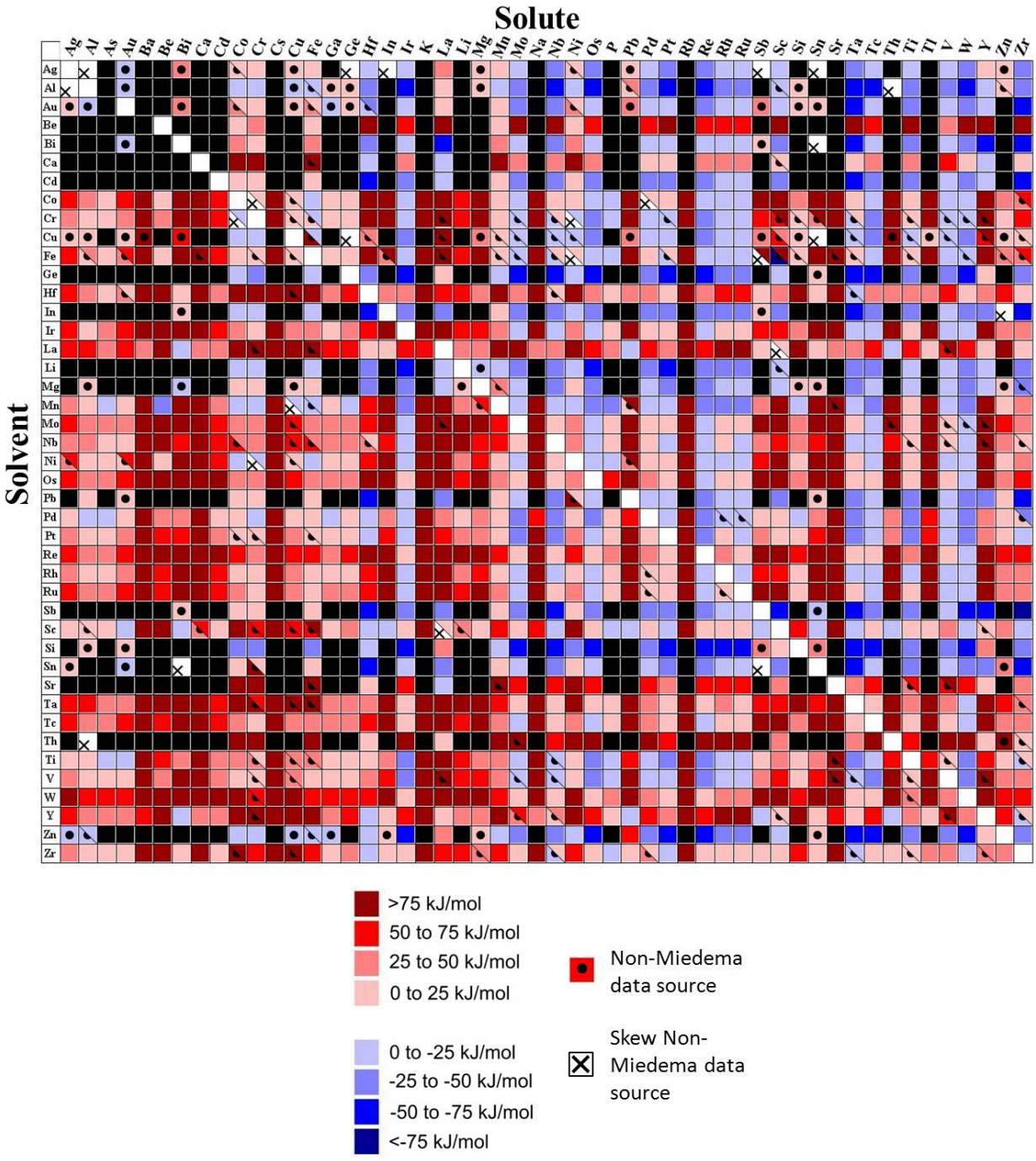

FIG 1 Segregation enthalpies for binary systems. Red scale (positive values) represents tendency for solute to segregate to the grain boundary. Blue scale describes anti-segregation (depletion of solute in grain boundary). Black indicates lack of data for the calculation. A dot indicates non-Miedema data sources, while an "x" indicates that these sources could not be used for the segregation calculation.

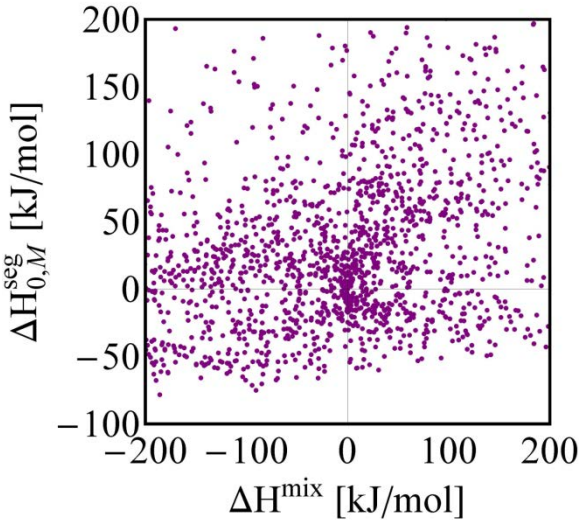

FIG 2. Enthalpies calculated using Eq. (8) for ΔH^{mix} and Eq. (10) for $\Delta H_{0,M}^{seg}$, for about 2500 binary metal pairs

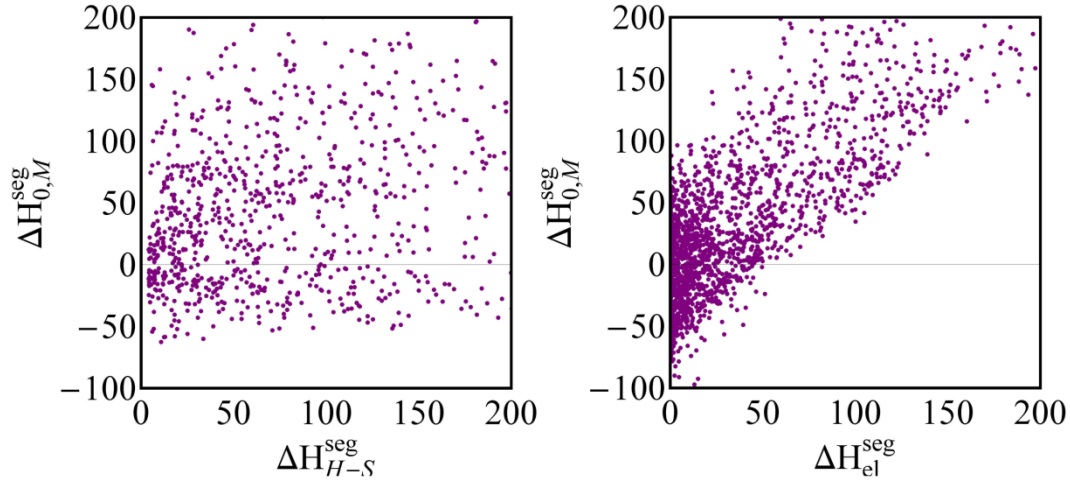

FIG. 3 A comparison of our segregation model, $\Delta H_{0,M}^{seg}$, with the Hondros-Seah model (ΔH_{H-S}^{seg}) and elastic-only enthalpy (ΔH_{el}^{seg}).

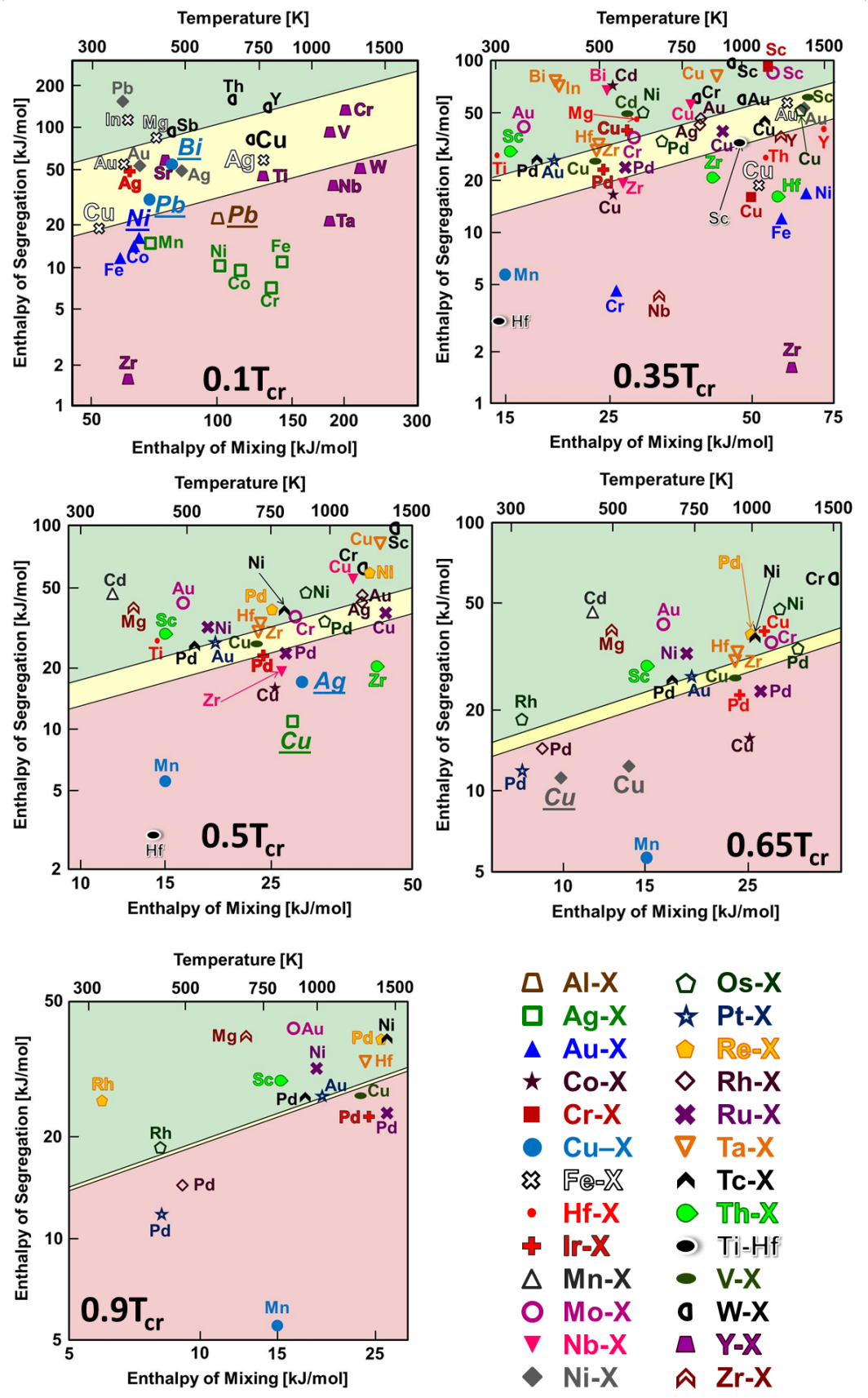
Temperature [K]
Enthalpy of Segregation [kJ/mol]
Enthalpy of Mixing [kJ/mol]
0.1T_cr
0.35T_cr
0.5T_cr
0.65T_cr
0.9T_cr
Al-X
Ag-X
Au-X
Co-X
Cr-X
Cu–X
Fe-X
Hf-X
Ir-X
Mn-X
Mo-X
Nb-X
Ni-X
Os-X
Pt-X
Re-X
Rh-X
Ru-X
Ta-X
Tc-X
Th-X
Ti-Hf
V-X
W-X
Y-X
Zr-X

FIG 4 Nanocrystalline Stability Maps for five fractional temperatures, with delineated regions of nanocrystalline stability (green, top), metastability (yellow, middle), and no stability (red, bottom). Alloys are represented by a symbol describing the solvent and a text label describing the solute.